
UniAttn: Reducing Inference Costs via Softmax Unification for Post-Training LLMs

Yizhe Xiong^{*1} Wei Huang^{*2} Xin Ye^{*3} Hui Chen¹ Zijia Lin¹ Haoran Lian⁴ Zhenpeng Su³ Jungong Han⁵
Guiguang Ding¹

Abstract

Post-training is essential for adapting Large Language Models (LLMs) to real-world applications. Deploying post-trained models faces significant challenges due to substantial memory overhead and noticeable inference latency. Existing work has identified significant redundancies in LLMs and proposed efficient architectures, namely intra-layer KV sharing and cross-layer KV sharing. However, these methods still result in high inference time overhead, remaining suboptimal for post-training pre-trained LLMs. In this paper, we identify that the `Softmax` operation is a primary bottleneck for LLM inference and discover that it is actually highly redundant during post-training. We propose Softmax **Unification in Attention (UniAttn)**, a novel post-training method that unifies Softmax activations across transformer blocks to reduce LLM inference costs. Additionally, UniAttn adopts a linear projection to compensate for the errors induced by Softmax unification. Experiments show that UniAttn matches the performance of standard post-training while significantly reducing inference costs, outperforming existing efficient architectures during post-training.

1. Introduction

Post-training (Lambert et al., 2024) has become a critical step in developing advanced LLMs for both general-purpose tasks (OpenAI, 2023; Liu et al., 2023) and domain-specific tasks (Thirunavukarasu et al., 2023; Wu et al., 2023; Shao et al., 2024). It typically refers to performing supervised fine-tuning (SFT) or domain-specific continual pre-training on pre-trained LLMs using a text corpus different from

the original pre-training dataset. Current post-training approaches for real-world applications involve fine-tuning popular base models (Dubey et al., 2024; Jiang et al., 2023; Rivière et al., 2024) with standard decoder-based architectures that have scaled to hundreds of billions of parameters. However, these approaches face two widely recognized challenges in deploying post-trained models (Xiao et al., 2024; Wang et al., 2024a; He et al., 2024; Brandon et al., 2024; Chen et al., 2024): (1) the substantial memory overhead required for KV-cache storage during inference, and (2) the computational latency, which leads to noticeable inference time.

To address those challenges, recent research has proposed KV-cache sharing methods, and showed that they offer notable advantages over traditional pruning (Ma et al., 2023; Zhang et al., 2023) and quantization (Xiao et al., 2023; Lin et al., 2024) methods: While pruning maintains model accuracy with only modest efficiency gains, and quantization reduces inference overhead at the expense of substantial performance degradation, KV-cache sharing methods achieve efficiency improvements with minimal performance drops. To this end, researchers have identified significant redundancies *inside and across LLM layers*, leading to two mainstream KV-cache sharing paradigms: intra-layer KV sharing, including MQA (Shazeer, 2019) and GQA (Ainslie et al., 2023), and a more aggressive cross-layer KV sharing, including CLA (Brandon et al., 2024) and YOCO (Sun et al., 2024). Despite achieving impressive KV-cache compression ratios, cross-layer KV sharing yields limited inference time reduction: less than 5% at deployment (see Section 4 for detailed results). This raises a critical question: *How to design LLM architectures that achieve both inference time and memory efficiency?*

To further explore that question, we delve deeper into LLM architectures and make two key observations. First, the *Softmax operation* significantly contributes to inference costs. Performing the Softmax operation requires access to the entire K-cache. Although the Softmax operation accounts for less than 1% of the total FLOPs compared to the linear projections in the backbone, it results in higher latency than the linear projections due to limited parallelism (Koo-

¹School of Software, Tsinghua University ²School of Computer Science, Beijing University of Posts and Telecommunications ³Kuaishou Technology ⁴Beihang University ⁵Department of Automation, Tsinghua University. Correspondence to: Yizhe Xiong <xiongyizhe2001@gmail.com>.

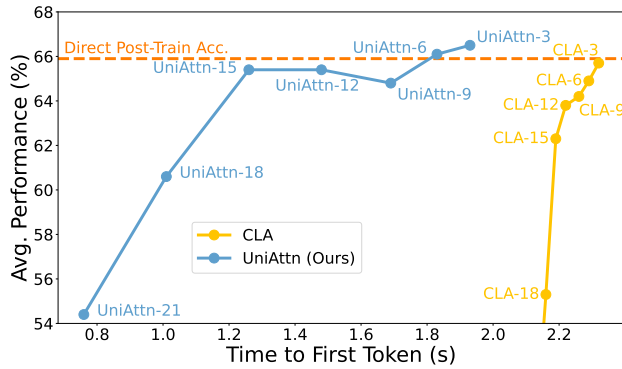


Figure 1. Comparisons of our UniAttn and directly applying cross-layer KV sharing (CLA) during post-training. “A-X” represents modifying total of X layers when applying A.

payegani & Pirsiavash, 2024; Liu et al., 2024). Second, *Softmax activations* exhibit high cross-layer similarity in the *top half layers* across various open-source pre-trained LLMs and post-training datasets. For instance, the average cross-layer similarity exceeds 0.9 on the top half layers in LLaMA-3.1 8B (Dubey et al., 2024) when evaluated on the Tulu3 (Lambert et al., 2024) training set (see Figure 2 for detailed results). This observation highlights the potential for an effective and generalizable approach to leveraging Softmax redundancies during post-training.

In this paper, we propose to post-train LLMs with Softmax **Unification in Attention (UniAttn)**. Specifically, we group consecutive transformer blocks in the LLM as several “Superblocks”, and unify the Softmax activations of all blocks within each Superblock. This approach significantly reduces memory and time costs. Additionally, we demonstrate that the error introduced by unifying Softmax activations can be effectively compensated by a linear projection, for which we design an initialization and training pipeline. To better interpret the performance gains of UniAttn, we present a theoretical analysis comparing it with existing cross-layer KV sharing methods. Our analysis reveals that UniAttn better preserves the benefits associated with model depth (Wang et al., 2024b), enabling the model to acquire new capabilities during post-training.

We conduct extensive experiments on four open-source pre-trained LLMs across two post-training scenarios: enhancing domain-specific capabilities and improving general capabilities. Our results show that UniAttn consistently achieves performance comparable to standard post-training while reducing inference costs. Compared to existing KV-cache sharing baselines, UniAttn achieves better performance with substantially lower inference costs (see Figure 1 for an overview). Furthermore, our UniAttn can be combined with intra-layer KV sharing and KV-cache compression methods to further cut down the memory overhead, showing strong practicality for real-world applications.

Overall, we summarize our contribution as follows:

- We identify that the Softmax operations in pre-trained LLMs, although yielding high inference costs, exhibit significant redundancies as Softmax activations share high cross-layer similarities.
- Based on the observations, we propose Softmax **Unification in Attention (UniAttn)** for post-training LLMs. Specifically, we unify the Softmax activations across decoder blocks. Additionally, we leverage linear projection to compensate for the error from Softmax unification. We show theoretically that UniAttn better preserves model capabilities than compared baselines.
- Extensive experiments show that UniAttn achieves comparable performance to standard post-training while reducing inference costs, outperforming existing efficient architectures.

2. Related Works

2.1. Post-Training LLMs

Building frontier LLMs for real-world applications involves two crucial stages: pre-training and post-training. Since pre-training data and methodologies are often proprietary, the research community has extensively explored post-training upon open-source pre-trained LLMs (Dubey et al., 2024; Rivière et al., 2024; Jiang et al., 2023) to enhance their *general* or *domain-specific* capabilities for deployment (Lian et al., 2024). Post-training is typically performed on instruction-following or domain-specific datasets. Recently, various datasets have been curated to equip LLMs with specific abilities, including general instruction-following models (Teknium et al., 2024; Lambert et al., 2024; BAAI, 2024), medical QA models (Wu et al., 2023; Gururajan et al., 2024; Singhal et al., 2023), legal QA models (Huang et al., 2023; Zhou et al., 2024), and models with strong mathematical problem-solving capabilities (Liu & Low, 2023).

Existing research on post-training mainly focuses on creating specific datasets for equipping open-source LLMs with specific capabilities. Differently, we investigate the redundancies in pre-trained LLMs and leverage them for post-training inference-efficient LLMs.

2.2. Efficient KV Sharing Architectures

Unlike existing pruning and quantization approaches (Bolya et al., 2023; Xiong et al., 2024), efficient KV sharing architectures utilize structural redundancies to create inference-efficient model variants for deployment. Those architectures mainly fall into two categories: intra-layer KV sharing, including MQA (Shazeer, 2019) and GQA (Ainslie et al., 2023), and cross-layer KV sharing, including CLA (Brandon et al., 2024) and YOCO (Sun et al., 2024). Specifically,

MQA (Shazeer, 2019) simplifies the attention mechanism by utilizing multiple query heads and a single KV head. GQA (Ainslie et al., 2023) takes a step further from MQA by organizing query heads as multiple groups and assigns different KV heads to each group. CLA (Brandon et al., 2024) proposes a cross-layer sharing mechanism to further reduce KV-cache memory overhead by sharing KV-cache across different layers. YOCO (Sun et al., 2024) transforms the original structure into self-decoders and cross-decoders, and adopts a global KV-cache across decoders.

Existing intra-layer KV sharing works have been adopted by various open-source LLMs (Dubey et al., 2024; Jiang et al., 2023; Rivière et al., 2024), yielding modest reduction on inference memory overhead. Although cross-layer KV sharing introduces more aggressive memory reduction, according to our analysis in Section 1 and Section 3.3, it still suffers from efficiency and performance issues. To address this, we propose UniAttn, which achieves promising performance for post-training LLMs and outperforms competing methods.

3. Methodology

3.1. Preliminaries

In this paper, we focus on mainstream decoder-only LLMs with a transformer structure. Each transformer block in an LLM features a multi-head self-attention (MHA) module and a feed-forward network (FFN). Given an input sequence $\mathbf{x} \in \mathbb{R}^{l \times d}$ where l denotes the sequence length and d denotes the hidden size, both MHA and FFN generate an output sequence with identical length and shape. We focus on the MHA module. Formally, we denote MHA output in layer i as \mathbf{x}'_i , where $\mathbf{x}'_i = \text{MHA}(\text{Norm}(\mathbf{x}_i)) + \mathbf{x}_i$. “Norm(\cdot)” denotes the Pre-Norm, a component adopted by mainstream open-source LLMs (Dubey et al., 2024; Jiang et al., 2023; Rivière et al., 2024; Bai et al., 2023). In the MHA module in layer i , each token in the input sequence \mathbf{x}_i is first projected by $W_{Q,i}$, $W_{K,i}$, and $W_{V,i}$, forming $Q_i, K_i \in d \times d_k$ and $V_i \in d \times d_v$. Then, the Softmax activation s_i is calculated by:

$$s_i = \text{softmax}\left(\frac{Q_i K_i^T}{\sqrt{d_k}}\right). \quad (1)$$

Subsequently, s_i is projected using V_i and the output weight matrix $W_{o,i}$ of the i th layer, and the input to MHA is added back through a residual connection to produce the MHA output \mathbf{x}'_i :

$$\mathbf{x}'_i = s_i V_i W_{o,i} + \mathbf{x}_i \quad (2)$$

3.2. UniAttn: Softmax Unification in Attention

Although existing KV-cache sharing methods—such as intra-layer and cross-layer KV sharing—can reduce the memory footprint, they offer limited inference time reduction. To

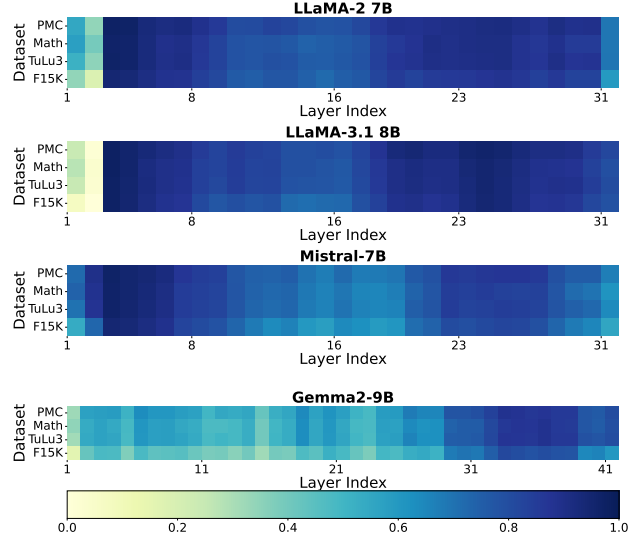


Figure 2. Cosine similarity results of average Softmax activations. Across all settings, the average Softmax activations of the top half of layers (i.e., the right half of each heatmap bar) share a high cosine similarity.

achieve both memory-efficiency and inference acceleration, we investigate the Softmax operation because (1) calculating Softmax demands the entire K-cache that accounts for 50% memory of the KV-cache; and (2) multiple studies (Geng et al., 2018; Koochpayegani & Pirsiavash, 2024) have recognized that the Softmax operation leads to high inference latency. We study the redundancy of Softmax activations in pre-trained LLMs by measuring the importance of Softmax operations in each layer. To ensure the generalizability of our study, we employ post-training datasets PMC (Wu et al., 2023), Infinity Instruct (Math) (BAAI, 2024), Tulu3 (Lambert et al., 2024), and long samples (F15K) provided by (Su, 2023), and utilize LLaMA-2 7B (Touvron et al., 2023), LLaMA-3.1 8B (Dubey et al., 2024), Mistral 7B (Jiang et al., 2023), and Gemma-2 9B (Rivière et al., 2024). We collect all Softmax activations, i.e., the s_i vectors in Equation (1), and compute the cosine similarity $\text{Sim}(i) = \cos(s_i, s_{i-1})$ for each sequence. We then average $\text{Sim}(i)$ over all sequences.

Observation: As shown in Figure 2, Softmax activations in *top half layers* share a high cross-layer similarity across different settings, showing that Softmax operations are highly redundant in LLMs. See Section C for quantitative analysis.

Motivated by such redundancy, we propose Softmax **Unification in Attention (UniAttn)** for post-training LLMs. Specifically, UniAttn groups consecutive decoder blocks in LLMs as “Superblocks”, and unifies the Softmax activations inside each Superblock to reduce the full Softmax operations and KV-cache size during inference. Additionally, we observe that the error introduced by Softmax unification can be compensated by a linear projection, and in turn design a

pipeline to initialize and train the linear projection. UniAttn simultaneously reduces the GPU memory and inference latency while achieving competitive performance. Different from cross-layer KV sharing, UniAttn does not diminish the “depth factor”. We show this in Section 3.4.

Unify Softmax Activations in Superblocks. To apply UniAttn, we first merge several consecutive transformer blocks as “SuperBlocks”. For simplicity, we create SuperBlocks of the same size. Inside each SuperBlock, only the bottom block employs the Softmax operation. Other blocks simply re-use the Softmax activation matrix s calculated by the bottom block in the SuperBlock. Formally, for layer $i + b$ that re-use the Softmax activation s_i from layer i :

$$\mathbf{x}'_{i+b} = s_i V_{i+b} W_{o,i+b} + \mathbf{x}_{i+b} \quad (3)$$

Since only the bottom block contribute to calculating the Key projection, other blocks that reuse Softmax activations do not store their corresponding K-cache, leading to GPU memory-inefficiency. Moreover, removing Softmax calculations in those layers also contribute to inference latency reduction. Similar to cross-layer KV sharing, UniAttn is also orthogonal to intra-layer KV sharing. In Section 4, we employ pre-trained LLMs with GQA to evaluate UniAttn.

Linear Compensation. Simply unifying Softmax activations unavoidably introduces errors in the forward pass. Formally, the error ϵ in layer $i + b$ is:

$$\begin{aligned} \epsilon = \mathbf{x}'_{i+b} - \mathbf{x}_{i+b} &= (\mathbf{x}_{i+b}^{\text{ori}} - \mathbf{x}_{i+b}^{\text{uni}}) \\ &+ \left(\text{softmax}\left(\frac{Q_{i+b} K_{i+b}^T}{\sqrt{d_k}}\right) - s_i \right) V_{i+b} W_{o,i+b} \end{aligned} \quad (4)$$

where $\mathbf{x}_{i+b}^{\text{ori}}$ and $\mathbf{x}_{i+b}^{\text{uni}}$ denote the input to layer $i + b$ in the original model and the model with UniAttn applied, respectively. According to (Koochpayegani & Pirsiavash, 2024), calculating linear projections yield *significantly lower* latency compared to the Softmax operation. And thus we study the effectiveness of compensating ϵ with a linear projection matrix W_c . To compensate for ϵ , we apply W_c to each layer with unified Softmax activations as:

$$\mathbf{x}'_{i+b} = s_i V_{i+b} W_{o,i+b} + \mathbf{x}_{i+b} + \mathbf{x}_{i+b} W_{c,i+b} \quad (5)$$

To find a proper initialization for W_c in a training-free manner, we propose to directly compensate ϵ :

Theorem 3.1. *The initialization for W_c that incurs minimal error when compensating $\mathbb{E}(\epsilon)$ satisfies:*

$$W_c = V \Sigma^+ U^T \mathbb{E}(\epsilon), \quad (6)$$

where $U \Sigma V^T$ denotes the SVD decomposition of $\mathbb{E}(\mathbf{x}_{i+b})$, Σ^+ denotes the pseudoinverse of Σ .

We leave the proof in the Appendix. In practice, we forward a small portion of training data from the post-training

datasets, and use the average values $\bar{\mathbf{x}}_{i+b}$ and $\bar{\epsilon}$ as estimations of $\mathbb{E}(\mathbf{x}_{i+b})$ and $\mathbb{E}(\epsilon)$. Considering that compensating for errors in previous layers would influence the calculation in subsequent layers, we calculate the initialization of W_c bottom-up. Experiments on the F15K dataset (Su, 2023) with sequence length 5,120 show that, after linear compensation, the errors for LLaMA-2 7B and LLaMA-3.1 8B are reduced to 2.9% (11.09/382.87) and 6.4% (5.76/89.58) of the original errors without compensation, respectively. This clearly demonstrates the effectiveness of the linear compensation. Please refer to Section I for more theoretical insights on the linear compensation.

To better train the linear transformations, we adopt a two-stage post-train pipeline. In the first stage, we only fine-tune the W_c weights *with early stop* and keep other weights frozen. We then conduct a full fine-tuning in the second stage. We formalize a detailed pipeline in Algorithm 1 in the Appendix.

3.3. Theoretical Analysis on Existing Methods

Existing KV-cache sharing methods can be mainly categorized as intra-layer KV sharing and cross-layer KV sharing methods. Intra-layer KV sharing methods can be directly combined with UniAttn (see Section 4 for detailed results). While cross-layer KV sharing methods achieve a more aggressive memory reduction rate, through theoretical analysis, we show that it diminishes the impact of model depth on model activations through directly sharing the same KV-cache across layers. This negatively affects the capabilities of pre-trained models, as model depth is a critical factor in determining their overall performance (Wang et al., 2024b).

Existing research (Razzhigaev et al., 2024) has shown that LLM layers can be approximated as linear transformations. Together with the conclusion on training gradient dynamics (Xiong et al., 2020), we first give a reasonable assumption:

Assumption 3.2. In top layers of **pre-trained** Pre-Norm LLMs:

$$\mathbf{x}_{i+1} = \mathbf{x}_i + \delta_i, \quad \text{where } \|\delta_i\| \ll \|\mathbf{x}_i\|. \quad (7)$$

We define δ as the “depth factor” that model applies on activations for further discussion. δ represents the extent to which model depth influences activations. *Please refer to Section E for theoretical insights on proposing this assumption.*

Analysis on Cross-layer KV Sharing: We adopt Theorem 3.2 to analyze the cross-layer KV sharing architecture, in which KV-cache is shared across multiple consecutive layers. Suppose layer $i + 1$ shares the KV-cache from layer i , the MHA operation in layer $i + 1$ can be written as:

$$\mathbf{x}'_{i+1} = \text{softmax}\left(\frac{Q K_i^T}{\sqrt{d_k}}\right) V_i W_{o,i+1} + \mathbf{x}_{i+1}, \quad (8)$$

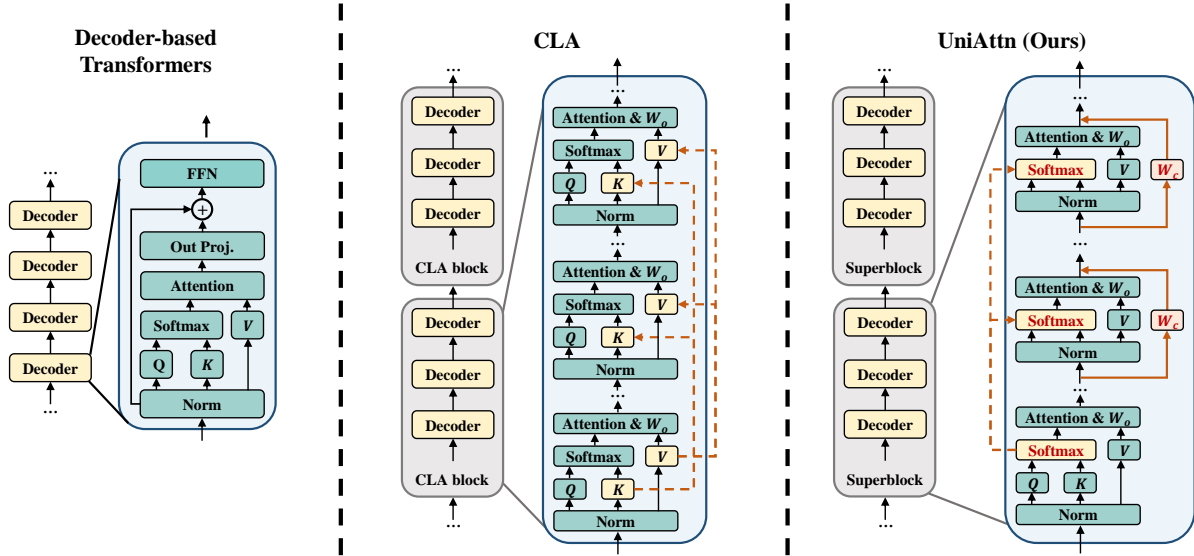


Figure 3. Pipeline comparison between standard decoder-based transformers, CLA (Brandon et al., 2024) (block size 3), and UniAttn (Superblock size 3). UniAttn shares the Softmax activations across layers in grouped Superblocks and adds linear transformation W_c to compensate for the unification error. For simplicity, only the self-attention calculation is illustrated for CLA and UniAttn.

where K_i and V_i are the K and V matrices from layer i . We propose that:

Proposition 3.3. *In pre-trained Pre-Norm LLMs, cross-layer KV sharing diminishes the “depth factor” δ on activations.*

Please refer to Section G for detailed proof. Theorem 3.3 gives a rigorous proof showing that cross-layer KV sharing diminishes the impact of model depth on model activations. To offer an intuitive understanding of how KV sharing alters the structure of QKV computation within self-attention, we reformulate the operation as follows:

$$\begin{aligned} \text{QKV-Comp}_{i+1} &= \text{softmax}(A_i)V_i \\ &= \text{softmax}\left(\frac{\mathbf{x}_i W_{q,i+1} K_i^T}{\sqrt{d_k}}\right)V_i. \end{aligned} \quad (9)$$

Compared to QKV-comp_i in the previous layer, the only difference lies in the use of distinct W_q matrices, suggesting that the QKV computation in layer $i + 1$ can be viewed as introducing an additional query head applied to the same KV pairs as in layer i . In this sense, *cross-layer KV sharing implicitly transforms QKV computation in different layers into additional query heads.*

3.4. Discussion on UniAttn

Our UniAttn reduces both memory cost and inference latency simultaneously. We underscore that unlike cross-layer KV sharing, our UniAttn does not diminish the “depth factor” δ in the forward pass. Please refer to Section H for detailed proof.

Proposition 3.4. *In pre-trained Pre-Norm LLMs, the “depth factor” in UniAttn is unignorable.*

4. Experiments

4.1. Experimental Settings

Post-Training Settings. We consider two post-training settings to validate our UniAttn: fine-tuning on domain-specific datasets and on general instruction following datasets. We choose PMC (Wu et al., 2023) as the domain-specific dataset and evaluate fine-tuned models on PubMedQA (Jin et al., 2019), MedMCQA (Pal et al., 2022), and MedQA (Jin et al., 2020). We choose Tulu3 (Lambert et al., 2024) as the general instruction following dataset and evaluate fine-tuned models on SIQA (Sap et al., 2019) and CommonsenseQA (Talmor et al., 2019). We employ (Gao et al., 2024) to perform all benchmark evaluations.

Model. We post-train 4 open-source pre-trained LLMs for evaluating our UniAttn: LLaMA-2 7B (Touvron et al., 2023), LLaMA-3.1 8B (Dubey et al., 2024), Mistral 7B (Jiang et al., 2023), and Gemma-2 9B (Rivière et al., 2024). We use base models that have undergone only pre-training.

Implementation details. We adopt the pattern in Figure 2 and apply UniAttn in the *top half* of layers. Unless otherwise noted, we adopt Superblock size = 4, which yields a total of 4 Superblocks in LLaMA-2 7B, LLaMA-3.1 8B, Mistral 7B, and 5 Superblocks in Gemma-2 9B. For all experiments, we post-train LLMs for 1 epoch (Lambert et al., 2024). We adopt all training hyperparameter values based

Method	TTFT (s)	KV Cache	Medical				General		
			PubMedQa	MedMCQA	MedQA	AVG	SIQA	CommonsenseQA	AVG
LLama3.1-8B (w/ GQA)									
Pre-Trained	2.33	100%	75.0	56.8	59.1	63.6	46.8	71.7	59.3
Post-Train	2.33	100%	75.4	59.0	63.2	65.9	50.1	73.9	62.0
LLMDrop-Half	1.77	81.3%	75.6	<u>57.8</u>	<u>61.5</u>	<u>65.0</u>	51.4	<u>75.0</u>	<u>63.2</u>
LLMDrop-Full	1.47	62.5%	<u>78.2</u>	53.6	55.9	62.6	51.8	73.3	62.6
CLA-Half	2.29	81.3%	73.8	58.1	62.8	64.9	<u>51.7</u>	74.7	<u>63.2</u>
CLA-Full	2.22	62.5%	75.4	56.9	59.2	63.8	50.7	71.2	61.0
UniAttn (Ours)	<u>1.48</u>	81.3%	79.0	57.6	59.5	65.4	51.1	75.6	63.4
LLama2-7B (w/o GQA)									
Pre-Trained	2.20	100%	71.4	32.2	34.7	46.1	50.2	51.1	52.7
Post-Train	2.20	100%	75.4	48.8	49.2	57.8	51.6	66.3	59.0
LLMDrop-Half	1.74	81.3%	<u>75.2</u>	48.4	49.8	<u>57.8</u>	<u>51.7</u>	<u>66.7</u>	<u>59.2</u>
LLMDrop-Full	1.37	62.5%	75.0	<u>48.8</u>	48.8	57.5	51.2	65.2	58.2
CLA-Half	2.20	81.3%	74.4	48.4	50.6	<u>57.8</u>	51.3	66.1	58.7
CLA-Full	2.23	62.5%	<u>75.2</u>	45.7	47.5	56.1	50.2	65.6	57.9
UniAttn (Ours)	<u>1.44</u>	81.3%	75.6	49.4	<u>50.1</u>	58.4	51.9	67.7	59.8

Table 1. Post-training performance (%) comparison. **Bold** and underline denote the best and second-best performance of compressed models. We also report time to first token (TTFT) and KV-cache retain rate (KV Cache).

on existing research. All training experiments were conducted on 8 H800 GPUs. For time to first token (TTFT) time measurement, we use a single H800 GPU and a context length of 8,192 and measure the time to generate the first token after receiving the sequence input. See the Appendix for more details.

4.2. Performance Comparison on Post-Training

We verify the effectiveness of UniAttn on 2 open-source LLMs with different architectures, namely LLaMA-3.1 8B (with GQA) (Dubey et al., 2024) and LLaMA-2 7B (without GQA) (Touvron et al., 2023). We use LLMDrop (He et al., 2024) and CLA (Brandon et al., 2024) as competing efficient architectures, as both methods exploit the cross-layer redundancies in LLMs. For LLMDrop, we bypass the MHA modules with the highest input-output similarities in the top half of the layers. For CLA, we group the top half of the layers into CLA blocks, using the same configuration as in the grouping of Superblocks. Since both competing methods drop the entire KV-cache in the operated layers, we compare two configurations: one with the same operating layers (X-Full) and another with the same KV-cache compression ratio (half operating layers, X-Half). We also conduct post-training after applying these methods. Same conclusions are observed on Mistral 7B (Jiang et al., 2023) and Gemma-2 9B (Rivière et al., 2024). Detailed results are in the Appendix due to the page limit.

Main Conclusion. We compare different efficient architectures against directly post-training the original LLM (Post-Train) and using the pre-trained model (Pre-Trained) as baselines, as shown in Table 1. Among all competing archi-

tectures, our UniAttn achieves the best overall performance across model structures (with and without GQA) and post-training datasets. Besides significantly reducing inference costs in both time and memory, UniAttn maintains comparable performance to directly post-training the original model, well demonstrating its effectiveness. When comparing UniAttn with LLMDrop-Full, we observe that Softmax unification provides a similar acceleration rate to bypassing the entire MHA module, but it achieves significantly better post-training performance. This aligns with our finding that Softmax operations are both costly and redundant. When comparing to CLA, UniAttn achieves better performance with significantly lower inference latency, demonstrating that the UniAttn architecture is better suited for post-training than cross-layer KV sharing.

Analysis of CLA. Since CLA only reduces the latency associated with KV projections, its impact on TTFT is minimal. As a result, CLA-Half, CLA-Full, and the original model exhibit comparable TTFT times. Furthermore, CLA achieves comparable performance to LLMDrop when applied to the same number of layers. This suggests that the cross-layer attention mechanism employed by CLA is structurally equivalent to directly bypassing the MHA module. This observation supports our theoretical analysis that cross-layer KV sharing methods like CLA can diminish the depth factor in pre-trained LLMs, limiting their performance.

4.3. Experimental Analysis

We choose LLaMA-3.1 8B (Dubey et al., 2024) and the medical domain to conduct experimental analysis. See Section C for more analysis.

UniAttn: Reducing Inference Costs via Softmax Unification for Post-Training LLMs

Method	Unify Softmax	Compensation	Init W_c	PubMed	MedMCQA	MedQA	AVG
Post-Train	-	-	-	75.4	59.0	63.2	65.9
UniAttn	✓	×	×	77.0	55.7	<u>58.8</u>	63.8
	✓	✓	zero-init	78.0	55.8	58.1	63.9
	✓	✓	Theorem 3.1	78.2	57.1	58.4	64.6
	✓	✓	Theorem 3.1 + fine-tune	79.0	57.6	59.5	65.4

Table 2. Ablation study results. **Bold** and underline denote the best and second-best UniAttn performance.

Method	TTFT (s)	H ₂ O Comp.	KV-Cache	AVG
Post-Train	2.33	-	100%	65.9
CLA-Half	2.29	-	81.3%	64.9
CLA-Full	2.22	-	62.5%	63.8
UniAttn	1.48	-	81.3%	65.4
	1.48	20%	65.0%	65.2
UniAttn+H ₂ O	1.46	40%	48.8%	65.0
	1.46	60%	32.5%	63.3

Table 3. Results of inference costs analysis. “H₂O Comp.” denotes the compression rate introduced by H₂O and “KV-Cache” denotes the KV-Cache retain rate.

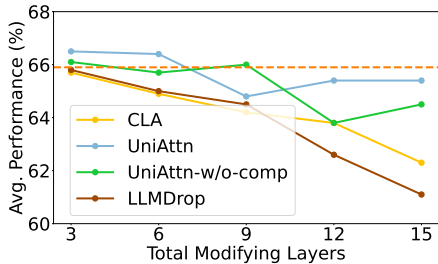


Figure 4. Comparison between baselines, UniAttn, and UniAttn without (“w/o”) linear compensation.

Ablation Studies. We do controlled experiments to evaluate the impact of each component in UniAttn, namely Softmax unification, linear compensation W_c , and the initialization for W_c . The results are shown in Table 2. We observe that after unifying the Softmax activations, both adding linear compensation and using proper initialization contribute positively to the final performance. While linear compensation consistently improves performance across different initialization methods, appropriate initialization proves critical for effectively fine-tuning W_c .

Inference Costs Analysis. We evaluate and compare inference costs to demonstrate the efficiency of UniAttn. To further maximize its potential, we integrate UniAttn with the KV-cache compression method H₂O (Zhang et al., 2023) to further reduce memory overhead by keeping only the essential and the recent tokens in the KV-cache. We report the TTFT latency and the total KV-cache retain rate. As shown in Table 3, UniAttn achieves a significant reduction in TTFT latency compared to CLA under the same KV-cache retain

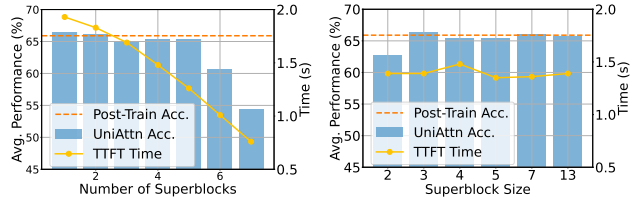


Figure 5. Hyperparameter analysis results on average accuracy (%) and TTFT latency (s). Left: Different total numbers of grouped Superblocks (each with size 4). Right: Different Superblock sizes (total of 12 layers that utilize unified Softmax activation).

rate. When combined with H₂O, UniAttn+H₂O reduces the KV-cache retain rate to below 50% while maintaining an average performance of 65.0%, achieving both better performance, lower inference latency, and higher KV-cache compression rate than CLA. These results clearly demonstrate the inference efficiency of UniAttn, highlighting its substantial benefits for real-world deployment scenarios.

Plain Softmax Unification v.s. Baselines. To further substantiate the theoretical analysis and demonstrate the effectiveness of Softmax unification, we compare UniAttn (without linear compensation, UniAttn-w/o-comp) against CLA and LLMDrop. As shown in Figure 4, simply unifying Softmax activations yields notable improvements over baselines, highlighting its core contribution. The linear projection serves as an enhancement, bringing UniAttn closer to post-train-level results.

Hyperparameter Analysis. We perform a hyperparameter analysis on the number and the size of Superblocks to evaluate their impact on latency and post-training performance. First, we examine the effect of varying the number of Superblocks. Using a consistent Superblock size of 4, we group different numbers of Superblocks from the top layers to the bottom layers. For instance, grouping 2 Superblocks indicates that layer 25-28 and 29-32 form the two Superblocks. The results are shown in Figure 5 (left). From the perspective of TTFT latency, increasing the number of Superblocks significantly reduces latency. From the perspective of performance, while grouping certain top layers as Superblocks does not substantially affect model performance, continuing to increase the number of Superblocks leads to sharp performance drops. Second, we analyze the impact of Superblock size. For fair comparison, we main-

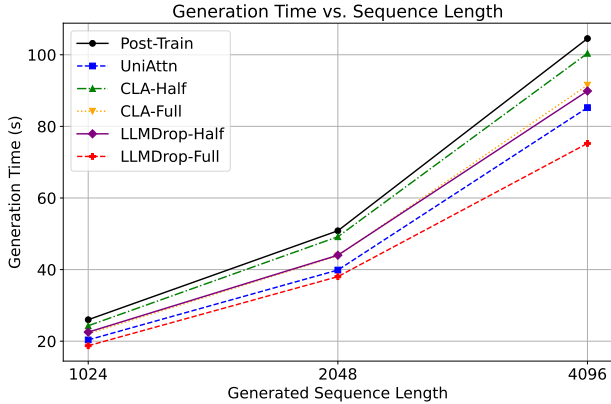


Figure 6. Generation efficiency (wall-clock time seconds) comparison on LLaMA-3.1 8B with 8192 context length.

Method	Sequence Length				AVG
	4096	8192	16384	32768	
Pre-Trained	82.67	0	0	0	20.67
Post-Train	<u>86.67</u>	87	80.33	72	81.5
LLMDrop-Half	87	83.67	77.67	68.67	79.25
CLA-Half	<u>86.67</u>	85.67	78.67	69.33	80.08
UniAttn (Ours)	87	<u>86.67</u>	<u>79.67</u>	<u>70.33</u>	<u>80.92</u>

Table 4. Post-training performance (%) comparison on Niah Multikey in RULER (Hsieh et al., 2024). **Bold** and underline denote the best and second-best performance.

tain a consistent total number of layers that utilize unified Softmax activations from preceding layers as 12. Since a Superblock with size b unifies Softmax in $b - 1$ layers, we set b such that $b - 1$ is a factor of 12, resulting in Superblock sizes of 2, 3, 4, 5, 7, and 13, and number of Superblocks as 12, 6, 4, 3, 2, and 1, respectively. As shown in Figure 5 (right), the size of the Superblocks does not significantly affect post-training performance. For simplicity, we use a Superblock size of 4, although fine-grained tuning of Superblock size could further improve post-training performance.

Generation Efficiency Analysis. To further analyze inference efficiency, we present the generation results of UniAttn against the comparing baselines, namely CLA-Half, CLA-Full, LLMDrop-Half, and LLMDrop-Full. We measure the end-to-end generation time with the LLaMA-3.1 8B backbone, and with generating 1024, 2048, and 4096 tokens using a context length of 8192. As shown in Figure 6, across all comparing methods, UniAttn consistently achieves Top-2 latency, only slightly behind LLMDrop-Full where all operated layers are simply skipped. These results demonstrate that unifying Softmax operations can substantially reduce the inference overhead during generation.

Generalization to Long-Context Modeling. To further validate the effectiveness of UniAttn on long context modeling

Method	Grouping	PubMed	MedMCQA	MedQA	AVG
Post-Train	-	75.4	59.0	63.2	65.9
UniAttn	Fixed size (4)	79.0	57.6	<u>59.5</u>	65.4
	Adaptive	78.8	57.3	59.5	65.2

Table 5. Performance (%) comparison of different Superblock grouping methods in UniAttn. **Bold** denotes the best performance.

scenarios, we follow the training recipe of (Bai et al., 2024) and post-train LLaMA-2 7B, which lacks native support for extended contexts. We compare UniAttn with two strong baselines, CLA-Half and LLMDrop-Half, on the Niah Multikey task in the RULER benchmark (Hsieh et al., 2024). To successfully implement long-context modeling, here we conduct experiments with *FlashAttention* (Dao et al., 2022) applied. As shown in Table 4, UniAttn consistently ranks in the top two (second only to full post-training) and outperforms all competing methods, well demonstrating its strong generalization ability to complex long-context tasks. This also suggests that our UniAttn is compatible with common acceleration frameworks such as FlashAttention.

Adaptive Superblock Grouping Schedule. To further investigate layerwise redundancy-aware grouping, we performed an additional experiment using a similarity-based adaptive scheme. We controlled the total number of “grouped layers” and assigned Superblocks by cosine similarity of layerwise Softmax activations. As shown in Table 5, for LLaMA-3.1 8B on the medical domain, this similarity-based grouping variant achieved comparable performance to setting the Superblock size as a fixed number, indicating that the performance of UniAttn is robust to different grouping strategies, and that adaptive grouping does not yield meaningful gains over the simpler fixed-size design.

5. Conclusion

In this work, we explored LLM redundancies and efficient architectures in the context of post-training to reduce the inference costs of LLMs. While existing KV-cache sharing methods successfully reduce the memory overhead, they yield limited inference time reduction during deployment. To address this limitation, we investigated the primary bottleneck in LLMs, the Softmax operation, and discovered significant redundancies across various pre-trained LLMs and datasets. Based on these findings, we proposed UniAttn, an efficient architecture that leverages these redundancies while preserving LLM capabilities through linear compensation in post-training. We further support UniAttn with a theoretical analysis, demonstrating its advantage over baselines. Extensive experiments on a series of models and datasets validate the effectiveness of UniAttn. Our UniAttn is particularly well-suited for real-world deployments, enjoying faster inference and less memory cost.

Impact Statement

This paper presents work whose goal is to advance the field of Machine Learning. There are many potential societal consequences of our work, none of which we feel must be specifically highlighted here.

References

- Ainslie, J., Lee-Thorp, J., de Jong, M., Zemlyanskiy, Y., Lebrón, F., and Sanghai, S. GQA: training generalized multi-query transformer models from multi-head checkpoints. In Bouamor, H., Pino, J., and Bali, K. (eds.), *Proceedings of the 2023 Conference on Empirical Methods in Natural Language Processing, EMNLP 2023, Singapore, December 6-10, 2023*, pp. 4895–4901. Association for Computational Linguistics, 2023. doi: 10.18653/V1/2023.EMNLP-MAIN.298. URL <https://doi.org/10.18653/v1/2023.emnlp-main.298>.
- BAAI. Infinity instruct, 2024. URL <https://github.com/FlagOpen/Infinity-Instruct>.
- Bai, J., Bai, S., Chu, Y., Cui, Z., Dang, K., Deng, X., Fan, Y., Ge, W., Han, Y., Huang, F., et al. Qwen technical report. *arXiv preprint arXiv:2309.16609*, 2023.
- Bai, Y., Lv, X., Zhang, J., He, Y., Qi, J., Hou, L., Tang, J., Dong, Y., and Li, J. LongAlign: A recipe for long context alignment of large language models. In *Findings of the Association for Computational Linguistics: EMNLP 2024*, pp. 1376–1395, Miami, Florida, USA, November 2024. Association for Computational Linguistics. doi: 10.18653/v1/2024.findings-emnlp.74. URL <https://aclanthology.org/2024.findings-emnlp.74>.
- Bolya, D., Fu, C., Dai, X., Zhang, P., Feichtenhofer, C., and Hoffman, J. Token merging: Your vit but faster. In *The Eleventh International Conference on Learning Representations, ICLR 2023, Kigali, Rwanda, May 1-5, 2023*. OpenReview.net, 2023. URL <https://openreview.net/forum?id=JroZRarw7Eu>.
- Brandon, W., Mishra, M., Nrusimha, A., Panda, R., and Ragan-Kelley, J. Reducing transformer key-value cache size with cross-layer attention. *CoRR*, abs/2405.12981, 2024. doi: 10.48550/ARXIV.2405.12981. URL <https://doi.org/10.48550/arXiv.2405.12981>.
- Chen, L., Zhao, H., Liu, T., Bai, S., Lin, J., Zhou, C., and Chang, B. An image is worth 1/2 tokens after layer 2: Plug-and-play inference acceleration for large vision-language models. In Leonardis, A., Ricci, E., Roth, S., Russakovsky, O., Sattler, T., and Varol, G. (eds.), *Computer Vision - ECCV 2024 - 18th European Conference, Milan, Italy, September 29-October 4, 2024, Proceedings, Part LXXXI*, volume 15139 of *Lecture Notes in Computer Science*, pp. 19–35. Springer, 2024. doi: 10.1007/978-3-031-73004-7_2. URL https://doi.org/10.1007/978-3-031-73004-7_2.
- Dao, T., Fu, D., Ermon, S., Rudra, A., and Ré, C. Flashattention: Fast and memory-efficient exact attention with io-awareness. *Advances in neural information processing systems*, 35:16344–16359, 2022.
- Dubey, A., Jauhri, A., Pandey, A., Kadian, A., Al-Dahle, A., Letman, A., Mathur, A., Schelten, A., Yang, A., Fan, A., Goyal, A., Hartshorn, A., Yang, A., Mitra, A., Srivankumar, A., Korenev, A., Hinsvark, A., Rao, A., Zhang, A., Rodriguez, A., Gregerson, A., Spataru, A., Rozière, B., Biron, B., Tang, B., Chern, B., Caucheteux, C., Nayak, C., Bi, C., Marra, C., McConnell, C., Keller, C., Touret, C., Wu, C., Wong, C., Ferrer, C. C., Nikolaidis, C., Allonsius, D., Song, D., Pintz, D., Livshits, D., Esiobu, D., Choudhary, D., Mahajan, D., Garcia-Olano, D., Perino, D., Hupkes, D., Lakomkin, E., AlBadawy, E., Lobanova, E., Dinan, E., Smith, E. M., Radenovic, F., Zhang, F., Synnaeve, G., Lee, G., Anderson, G. L., Nail, G., Mialon, G., Pang, G., Cucurell, G., Nguyen, H., Korevaar, H., Xu, H., Touvron, H., Zarov, I., Ibarra, I. A., Kloumann, I. M., Misra, I., Evtimov, I., Copet, J., Lee, J., Geffert, J., Vranes, J., Park, J., Mahadeokar, J., Shah, J., van der Linde, J., Billock, J., Hong, J., Lee, J., Fu, J., Chi, J., Huang, J., Liu, J., Wang, J., Yu, J., Bitton, J., Spisak, J., Park, J., Rocca, J., Johnston, J., Saxe, J., Jia, J., Alwala, K. V., Upasani, K., Plawiak, K., Li, K., Heafield, K., Stone, K., and et al. The llama 3 herd of models. *CoRR*, abs/2407.21783, 2024. doi: 10.48550/ARXIV.2407.21783. URL <https://doi.org/10.48550/arXiv.2407.21783>.
- Fearnley, J. and Savani, R. The complexity of the simplex method. In *Proceedings of the forty-seventh annual ACM symposium on Theory of computing*, pp. 201–208, 2015.
- Gao, L., Tow, J., Abbasi, B., Biderman, S., Black, S., DiPofi, A., Foster, C., Golding, L., Hsu, J., Le Noac’h, A., Li, H., McDonell, K., Muennighoff, N., Ociepa, C., Phang, J., Reynolds, L., Schoelkopf, H., Skowron, A., Sutawika, L., Tang, E., Thite, A., Wang, B., Wang, K., and Zou, A. A framework for few-shot language model evaluation, 07 2024. URL <https://zenodo.org/records/12608602>.
- Geng, X., Lin, J., Zhao, B., Kong, A., Aly, M. M. S., and Chandrasekhar, V. Hardware-aware softmax approximation for deep neural networks. In Jawahar, C. V., Li, H., Mori, G., and Schindler, K. (eds.), *Computer Vision - ACCV 2018 - 14th Asian Conference on Computer Vision, Perth, Australia, December 2-6, 2018, Revised Se-*

- lected Papers, Part IV*, volume 11364 of *Lecture Notes in Computer Science*, pp. 107–122. Springer, 2018. doi: 10.1007/978-3-030-20870-7_7. URL https://doi.org/10.1007/978-3-030-20870-7_7.
- Gururajan, A. K., Lopez-Cuena, E., Bayarri-Planas, J., Tormos, A., Hinjos, D., Bernabeu-Perez, P., Arias-Duart, A., Martin-Torres, P. A., Urcelay-Ganzabal, L., Gonzalez-Mallo, M., Alvarez-Napagao, S., Ayguadé-Parra, E., and Garcia-Gasulla, U. C. D. Aloe: A family of fine-tuned open healthcare llms, 2024. URL <https://arxiv.org/abs/2405.01886>.
- He, S., Sun, G., Shen, Z., and Li, A. What matters in transformers? not all attention is needed. *CoRR*, abs/2406.15786, 2024. doi: 10.48550/ARXIV.2406.15786. URL <https://doi.org/10.48550/arXiv.2406.15786>.
- Hsieh, C.-P., Sun, S., Krizan, S., Acharya, S., Rekish, D., Jia, F., Zhang, Y., and Ginsburg, B. Ruler: What’s the real context size of your long-context language models? *arXiv preprint arXiv:2404.06654*, 2024.
- Huang, Q., Tao, M., Zhang, C., An, Z., Jiang, C., Chen, Z., Wu, Z., and Feng, Y. Lawyer llama technical report, 2023. URL <https://arxiv.org/abs/2305.15062>.
- Jiang, A. Q., Sablayrolles, A., Mensch, A., Bamford, C., Chaplot, D. S., de Las Casas, D., Bressand, F., Lengyel, G., Lample, G., Saulnier, L., Lavaud, L. R., Lachaux, M., Stock, P., Scao, T. L., Lavril, T., Wang, T., Lacroix, T., and Sayed, W. E. Mistral 7b. *CoRR*, abs/2310.06825, 2023. doi: 10.48550/ARXIV.2310.06825. URL <https://doi.org/10.48550/arXiv.2310.06825>.
- Jin, D., Pan, E., Oufattole, N., Weng, W., Fang, H., and Szolovits, P. What disease does this patient have? A large-scale open domain question answering dataset from medical exams. *CoRR*, abs/2009.13081, 2020. URL <https://arxiv.org/abs/2009.13081>.
- Jin, Q., Dhingra, B., Liu, Z., Cohen, W. W., and Lu, X. Pubmedqa: A dataset for biomedical research question answering. In Inui, K., Jiang, J., Ng, V., and Wan, X. (eds.), *Proceedings of the 2019 Conference on Empirical Methods in Natural Language Processing and the 9th International Joint Conference on Natural Language Processing, EMNLP-IJCNLP 2019, Hong Kong, China, November 3-7, 2019*, pp. 2567–2577. Association for Computational Linguistics, 2019. doi: 10.18653/v1/D19-1259. URL <https://doi.org/10.18653/v1/D19-1259>.
- Koohpayegani, S. A. and Pirsiavash, H. Sima: Simple softmax-free attention for vision transformers. In *IEEE/CVF Winter Conference on Applications of Computer Vision, WACV 2024, Waikoloa, HI, USA, January 3-8, 2024*, pp. 2595–2605. IEEE, 2024. doi: 10.1109/WACV57701.2024.00259. URL <https://doi.org/10.1109/WACV57701.2024.00259>.
- Lambert, N., Morrison, J., Pyatkin, V., Huang, S., Ivison, H., Brahman, F., Miranda, L. J. V., Liu, A., Dziri, N., Lyu, S., Gu, Y., Malik, S., Graf, V., Hwang, J. D., Yang, J., Bras, R. L., Tafford, O., Wilhelm, C., Soldaini, L., Smith, N. A., Wang, Y., Dasigi, P., and Hajishirzi, H. Tulu 3: Pushing frontiers in open language model post-training. *CoRR*, abs/2411.15124, 2024. doi: 10.48550/ARXIV.2411.15124. URL <https://doi.org/10.48550/arXiv.2411.15124>.
- Lian, H., Chen, J., Huang, W., Xiong, Y., Hu, W., Ding, G., Chen, H., Niu, J., Lin, Z., Zhang, F., and Zhang, D. Breaking the stage barrier: A novel single-stage approach to long context extension for large language models, 2024. URL <https://arxiv.org/abs/2412.07171>.
- Lin, J., Tang, J., Tang, H., Yang, S., Chen, W.-M., Wang, W.-C., Xiao, G., Dang, X., Gan, C., and Han, S. Awq: Activation-aware weight quantization for llm compression and acceleration. In *MLSys*, 2024.
- Liu, H., Li, C., Wu, Q., and Lee, Y. J. Visual instruction tuning. In Oh, A., Naumann, T., Globerson, A., Saenko, K., Hardt, M., and Levine, S. (eds.), *Advances in Neural Information Processing Systems 36: Annual Conference on Neural Information Processing Systems 2023, NeurIPS 2023, New Orleans, LA, USA, December 10 - 16, 2023*, 2023. URL http://papers.nips.cc/paper_files/paper/2023/hash/6dcf277ea32ce3288914faf369fe6de0-Abstract-Conference.html.
- Liu, S., Tao, G., Zou, Y., Chow, D., Fan, Z., Lei, K., Pan, B., Sylvester, D., Kielian, G., and Saligane, M. Consmax: Hardware-friendly alternative softmax with learnable parameters. In *Proceedings of the 43rd IEEE/ACM International Conference on Computer-Aided Design*, pp. 1–9, 2024.
- Liu, T. and Low, B. K. H. Goat: Fine-tuned llama outperforms gpt-4 on arithmetic tasks, 2023. URL <https://arxiv.org/abs/2305.14201>.
- Ma, X., Fang, G., and Wang, X. Llm-pruner: On the structural pruning of large language models. In *Advances in Neural Information Processing Systems*, 2023.
- Men, X., Xu, M., Zhang, Q., Wang, B., Lin, H., Lu, Y., Han, X., and Chen, W. Shortgpt: Layers in large language models are more redundant than you expect. *CoRR*, abs/2403.03853, 2024. doi: 10.48550/ARXIV.2403.03853. URL <https://doi.org/10.48550/arXiv.2403.03853>.

- OpenAI. GPT-4 technical report. *CoRR*, abs/2303.08774, 2023. doi: 10.48550/ARXIV.2303.08774. URL <https://doi.org/10.48550/arXiv.2303.08774>.
- Pal, A., Umaphathi, L. K., and Sankarasubbu, M. Medmqa: A large-scale multi-subject multi-choice dataset for medical domain question answering. In Flores, G., Chen, G. H., Pollard, T. J., Ho, J. C., and Naumann, T. (eds.), *Conference on Health, Inference, and Learning, CHIL 2022, 7-8 April 2022, Virtual Event*, volume 174 of *Proceedings of Machine Learning Research*, pp. 248–260. PMLR, 2022. URL <https://proceedings.mlr.press/v174/pal22a.html>.
- Razhigayev, A., Mikhalchuk, M., Goncharova, E., Gerasimenko, N., Oseledets, I., Dimitrov, D., and Kuznetsov, A. Your transformer is secretly linear. In Ku, L.-W., Martins, A., and Srikumar, V. (eds.), *Proceedings of the 62nd Annual Meeting of the Association for Computational Linguistics (Volume 1: Long Papers)*, pp. 5376–5384, Bangkok, Thailand, August 2024. Association for Computational Linguistics. doi: 10.18653/v1/2024.acl-long.293. URL <https://aclanthology.org/2024.acl-long.293/>.
- Rivière, M., Pathak, S., Sessa, P. G., Hardin, C., Bhupatiraju, S., Hussenot, L., Mesnard, T., Shahriari, B., Ramé, A., Ferret, J., Liu, P., Tafti, P., Friesen, A., Casbon, M., Ramos, S., Kumar, R., Lan, C. L., Jerome, S., Tsitsulin, A., Vieillard, N., Stanczyk, P., Girgin, S., Momchev, N., Hoffman, M., Thakoor, S., Grill, J., Neyshabur, B., Bachem, O., Walton, A., Severyn, A., Parrish, A., Ahmad, A., Hutchison, A., Abdagic, A., Carl, A., Shen, A., Brock, A., Coenen, A., Laforge, A., Paterson, A., Bastian, B., Piot, B., Wu, B., Royal, B., Chen, C., Kumar, C., Perry, C., Welty, C., Choquette-Choo, C. A., Sinopalnikov, D., Weinberger, D., Vijaykumar, D., Rogozinska, D., Herbison, D., Bandy, E., Wang, E., Noland, E., Moreira, E., Senter, E., Eltyshv, E., Visin, F., Rasskin, G., Wei, G., Cameron, G., Martins, G., Hashemi, H., Klimczak-Plucinska, H., Batra, H., Dhand, H., Nardini, I., Mein, J., Zhou, J., Svensson, J., Stanway, J., Chan, J., Zhou, J. P., Carrasqueira, J., Iljazi, J., Becker, J., Fernandez, J., van Amersfoort, J., Gordon, J., Lipschultz, J., Newlan, J., Ji, J., Mohamed, K., Badola, K., Black, K., Millican, K., McDonell, K., Nguyen, K., Sodhia, K., Greene, K., Sjöstrand, L. L., Usui, L., Sifre, L., Heuermann, L., Lago, L., and McNealus, L. Gemma 2: Improving open language models at a practical size. *CoRR*, abs/2408.00118, 2024. doi: 10.48550/ARXIV.2408.00118. URL <https://doi.org/10.48550/arXiv.2408.00118>.
- Sap, M., Rashkin, H., Chen, D., Bras, R. L., and Choi, Y. Socialiqa: Commonsense reasoning about social interactions. *CoRR*, abs/1904.09728, 2019. URL <http://arxiv.org/abs/1904.09728>.
- Shao, Z., Wang, P., Zhu, Q., Xu, R., Song, J., Zhang, M., Li, Y. K., Wu, Y., and Guo, D. Deepseekmath: Pushing the limits of mathematical reasoning in open language models. *CoRR*, abs/2402.03300, 2024. doi: 10.48550/ARXIV.2402.03300. URL <https://doi.org/10.48550/arXiv.2402.03300>.
- Shazeer, N. Fast transformer decoding: One write-head is all you need, 2019. URL <https://arxiv.org/abs/1911.02150>.
- Singhal, K., Tu, T., Gottweis, J., Sayres, R., Wulczyn, E., Hou, L., Clark, K., Pfohl, S., Cole-Lewis, H., Neal, D., Schaeckermann, M., Wang, A., Amin, M., Lachgar, S., Mansfield, P., Prakash, S., Green, B., Dominowska, E., y Arcas, B. A., Tomasev, N., Liu, Y., Wong, R., Semturs, C., Mahdavi, S. S., Barral, J., Webster, D., Corrado, G. S., Matias, Y., Azizi, S., Karthikesalingam, A., and Natarajan, V. Towards expert-level medical question answering with large language models, 2023. URL <https://arxiv.org/abs/2305.09617>.
- Su, J. Rectified rotary position embeddings. <https://github.com/bojone/rerope>, 2023.
- Sun, Y., Dong, L., Zhu, Y., Huang, S., Wang, W., Ma, S., Zhang, Q., Wang, J., and Wei, F. You only cache once: Decoder-decoder architectures for language models. *CoRR*, abs/2405.05254, 2024. doi: 10.48550/ARXIV.2405.05254. URL <https://doi.org/10.48550/arXiv.2405.05254>.
- Talmor, A., Herzig, J., Lourie, N., and Berant, J. Commonsenseqa: A question answering challenge targeting commonsense knowledge. In Burstein, J., Doran, C., and Solorio, T. (eds.), *Proceedings of the 2019 Conference of the North American Chapter of the Association for Computational Linguistics: Human Language Technologies, NAACL-HLT 2019, Minneapolis, MN, USA, June 2-7, 2019, Volume 1 (Long and Short Papers)*, pp. 4149–4158. Association for Computational Linguistics, 2019. doi: 10.18653/v1/N19-1421. URL <https://doi.org/10.18653/v1/n19-1421>.
- Teknum, R., Quesnelle, J., and Guang, C. Hermes 3 technical report, 2024. URL <https://arxiv.org/abs/2408.11857>.
- Thirunavukarasu, A. J., Ting, D. S. J., Elangovan, K., Gutierrez, L., Tan, T. F., and Ting, D. S. W. Large language models in medicine. *Nature medicine*, 29(8):1930–1940, 2023.
- Touvron, H., Martin, L., Stone, K., Albert, P., Almahairi, A., Babaei, Y., Bashlykov, N., Batra, S., Bhargava, P., Bhosale, S., et al. Llama 2: Open foundation and fine-tuned chat models. *arXiv preprint arXiv:2307.09288*, 2023.

- Wang, A., Chen, H., Tan, J., Zhang, K., Cai, X., Lin, Z., Han, J., and Ding, G. Prefixkv: Adaptive prefix kv cache is what vision instruction-following models need for efficient generation, 2024a. URL <https://arxiv.org/abs/2412.03409>.
- Wang, H., Ma, S., Dong, L., Huang, S., Zhang, D., and Wei, F. Deepnet: Scaling transformers to 1,000 layers. *IEEE Trans. Pattern Anal. Mach. Intell.*, 46(10):6761–6774, 2024b. doi: 10.1109/TPAMI.2024.3386927. URL <https://doi.org/10.1109/TPAMI.2024.3386927>.
- Wu, C., Zhang, X., Zhang, Y., Wang, Y., and Xie, W. Pmc-llama: Further finetuning llama on medical papers. *CoRR*, abs/2304.14454, 2023. doi: 10.48550/ARXIV.2304.14454. URL <https://doi.org/10.48550/arXiv.2304.14454>.
- Xiao, G., Lin, J., Seznec, M., Wu, H., Demouth, J., and Han, S. SmoothQuant: Accurate and efficient post-training quantization for large language models. In *Proceedings of the 40th International Conference on Machine Learning*, 2023.
- Xiao, G., Tian, Y., Chen, B., Han, S., and Lewis, M. Efficient streaming language models with attention sinks. In *The Twelfth International Conference on Learning Representations, ICLR 2024, Vienna, Austria, May 7-11, 2024*. OpenReview.net, 2024. URL <https://openreview.net/forum?id=NG7sS51zVF>.
- Xiong, R., Yang, Y., He, D., Zheng, K., Zheng, S., Xing, C., Zhang, H., Lan, Y., Wang, L., and Liu, T. On layer normalization in the transformer architecture. In *Proceedings of the 37th International Conference on Machine Learning, ICML 2020, 13-18 July 2020, Virtual Event*, volume 119 of *Proceedings of Machine Learning Research*, pp. 10524–10533. PMLR, 2020. URL <http://proceedings.mlr.press/v119/xiong20b.html>.
- Xiong, Y., Chen, H., Hao, T., Lin, Z., Han, J., Zhang, Y., Wang, G., Bao, Y., and Ding, G. PYRA: parallel yielding re-activation for training-inference efficient task adaptation. In Leonardis, A., Ricci, E., Roth, S., Rusakovsky, O., Sattler, T., and Varol, G. (eds.), *Computer Vision - ECCV 2024 - 18th European Conference, Milan, Italy, September 29-October 4, 2024, Proceedings, Part IX*, volume 15067 of *Lecture Notes in Computer Science*, pp. 455–473. Springer, 2024. doi: 10.1007/978-3-031-72673-6_25. URL https://doi.org/10.1007/978-3-031-72673-6_25.
- Zhang, Z., Sheng, Y., Zhou, T., Chen, T., Zheng, L., Cai, R., Song, Z., Tian, Y., Ré, C., Barrett, C. W., Wang, Z., and Chen, B. H2O: heavy-hitter oracle for efficient generative inference of large language models. In Oh, A., Naumann, T., Globerson, A., Saenko, K., Hardt, M., and Levine, S. (eds.), *Advances in Neural Information Processing Systems 36: Annual Conference on Neural Information Processing Systems 2023, NeurIPS 2023, New Orleans, LA, USA, December 10 - 16, 2023*, 2023. URL http://papers.nips.cc/paper_files/paper/2023/hash/6ceefa7b15572587b78ecfceb2827f8-Abstract-Conference.html.
- Zhou, Z., Shi, J.-X., Song, P.-X., Yang, X.-W., Jin, Y.-X., Guo, L.-Z., and Li, Y.-F. Lawgpt: A chinese legal knowledge-enhanced large language model, 2024. URL <https://arxiv.org/abs/2406.04614>.

Method	Model	Learning Rate	Weight Decay	Batch Size	Epochs	Superblock Size	Superblock Groups
UniAttn	LLaMA-2 7B	2e-5	0	48	1	4	[17-20], [21-24], [25-28], [29-32]
	LLaMA-3.1 8B	7e-6	0	48	1	4	[17-20], [21-24], [25-28], [29-32]
	Mistral 7B	1e-6	0	48	1	4	[17-20], [21-24], [25-28], [29-32]
	Gemma-2 9B	1e-6	0	48	1	4	[22-25], [26-29], [30-33], [34-37], [38-41]

Table 6. Training hyperparameter details of UniAttn.

Method	Model	Learning Rate	Weight Decay	Batch Size	Epochs	CLA Block Size	CLA Block Groups
CLA-Half	LLaMA-2 7B	2e-5	0	48	1	4	[25-28], [29-32]
	LLaMA-3.1 8B	7e-6	0	48	1	4	[25-28], [29-32]
	Mistral 7B	1e-6	0	48	1	4	[25-28], [29-32]
	Gemma-2 9B	1e-6	0	48	1	4	[30-33], [34-37], [38-41]
CLA-Full	LLaMA-2 7B	2e-5	0	48	1	4	[17-20], [21-24], [25-28], [29-32]
	LLaMA-3.1 8B	7e-6	0	48	1	4	[17-20], [21-24], [25-28], [29-32]
	Mistral 7B	1e-6	0	48	1	4	[17-20], [21-24], [25-28], [29-32]
	Gemma-2 9B	1e-6	0	48	1	4	[22-25], [26-29], [30-33], [34-37], [38-41]

Table 7. Training hyperparameter details of CLA.

Method	Model	Learning Rate	Weight Decay	Batch Size	Epochs	# of Dropped Layers	Index of Dropped Layers
LLMDrop-Half	LLaMA-2 7B	2e-5	0	48	1	6	23,20,32,27,22,24
	LLaMA-3.1 8B	7e-6	0	48	1	6	19,22,20,21,27,23
	Mistral 7B	1e-6	0	48	1	6	17,32,31,21,22,24
	Gemma-2 9B	1e-6	0	48	1	8	29,26,21,30,27,40,38,31
LLMDrop-Full	LLaMA-2 7B	2e-5	0	48	1	12	23,20,32,27,22,24,31,29,25,30,28,26
	LLaMA-3.1 8B	7e-6	0	48	1	12	19,22,20,21,27,23,30,29,28,26,24,25
	Mistral 7B	1e-6	0	48	1	12	17,32,31,21,22,24,29,23,28,25,27,26
	Gemma-2 9B	1e-6	0	48	1	15	29,26,21,30,27,40,38,31,32,33,35,39,36,37,34

Table 8. Training hyperparameter details of LLMDrop. The index of dropped layers are ordered by input-output similarity.

A. License for Scientific Artifacts

The Training dataset PMC (Wu et al., 2023) is licensed under OpenRAIL license¹. The Training dataset TuLu3 (Lambert et al., 2024) is licensed under Open Data Commons License². The Mistral model (Jiang et al., 2023), Gemma-2 model (Rivière et al., 2024), LLaMA-2 (Huang et al., 2023) model, and LLaMA-3.1 model (Dubey et al., 2024) are licensed under Apache License 2.0³. The LongAlign evaluation dataset is also licensed under Apache License 2.0⁴. The evaluation datasets (Hsieh et al., 2024; Talmor et al., 2019; Sap et al., 2019; Jin et al., 2020; Pal et al., 2022; Jin et al., 2019) are subject to the MIT license⁵. All usages of scientific artifacts in this paper obey the corresponding licenses.

B. More Implementation Details for Reproducibility

Post-Training Datasets. Regarding the medical domain, we directly employ the instruction tuning dataset for PMC⁶ (Wu et al., 2023) (i.e., training stage-2 for PMC-LLaMA) for post-training. The dataset consists of 513,999 instruction-input-output pairs. Regarding the general instruction tuning scenario, we employ the Tulu 3 SFT Mixture⁷ and filter for data with only 1 round of conversation, resulting in 896,070 input-output pairs.

Training Hyperparameters. The training hyperparameters for all experiments are reported in table Table 6, Table 7 and Table 8. Note that we adopt the learning rate and weight decay values according to existing research, in which those

¹<https://www.licenses.ai/blog/2022/8/26/bigscience-open-rail-m-license>

²<https://opendatacommons.org/licenses/>

³<https://choosealicense.com/licenses/apache-2.0/>

⁴<https://choosealicense.com/licenses/apache-2.0/>

⁵<https://choosealicense.com/licenses/mit/>

⁶https://huggingface.co/datasets/axiong/pmc_llama_instructions

⁷<https://huggingface.co/datasets/allenai/tulu-3-sft-mixture>

Package	Version	Package	Version
PyTorch	2.0.0	transformers	4.46.0
deepspeed	0.10.0	tokenizers	0.20.1
datasets	2.14.3		

Table 9. Versions of used packages.

pre-trained models are post-trained under reported schedules.

Evaluation Details. For all experiments, we evaluate the final checkpoint after post-training for benchmark evaluation. Regarding the medical domain, we report the 0-shot result on both PubMed, MegMCQA, and MedQA datasets. Regarding the general instruction tuning scenario, we report 0-shot result on both SIQA and CommonsenseQA for LLaMA-3.1 8B, Mistral 7B, and Gemma-2 9B models. For the earlier-released LLaMA-2 7B model, since it has a shorter pre-training context length, we report its 5-shot result as Tulu 3 mainly enhances model performance with longer context.

Prompt for Post-Training. We employ the same prompt for post-training in both the medical domain and general instruction tuning scenario:

```
"Below is an instruction that
describes a task, paired with an input
that provides further context. Write a
response that appropriately completes
the request.\n\n###
Instruction:\n{instruction}\n\n###
Input:\n{input}\n\n###
Response: {output} <EOS_TOKEN>"
```

We simply keep the instruction field empty if no instruction is provided.

Experiment Packages. We report the version numbers of used packages in Table 9.

C. More Experiment Results

Main Results on Mistral 7B and Gemma-2 9B. We adopt the settings in Table 1 and conduct the same experiments on Mistral 7B (Jiang et al., 2023) and Gemma-2 9B (Rivière et al., 2024). The results are shown in Table 10. Consistent with the results on the LLaMA models, our UniAttn achieves the best overall performance on both LLMs and post-training datasets while significantly reducing both time and memory costs. When operating the same number of layers, UniAttn achieves similar TTFT time to LLMDrop, well demonstrating the effectiveness of Softmax activation unification. Although CLA and LLMDrop achieve competitive results in some settings (e.g., CLA-Half in post-training Gemma on general instruction datasets), *they cannot provide consistent performance across different settings*. Additionally, even on the Mistral and Gemma models, CLA achieves similar performance to its corresponding LLMDrop setting, again indicating that CLA diminishes the depth factor in pre-trained LLMs.

Quantitative Analysis of Softmax Redundancies. In Figure 2 of the main article, we observed that Softmax activations in *top half layers* share a high cross-layer similarity across different models and datasets. To provide a more comprehensive analysis, here we take LLaMA-3.1 8B as an example and present some statistics of the cosine similarity of Softmax activations. As shown in Table 11, cosine similarities appear to be consistent across different datasets, with average values ranging from 0.79 to 0.83. The maximum cosine similarity remains consistently high at 0.97, indicating that the overall range of cosine similarity remains stable across layers and datasets. The differences for cosine similarity between the top and bottom halves of layers indicate that Softmax operations are more redundant in deeper layers, as noted in the main article. The standard deviation values suggest that redundancy is fairly consistent across datasets. Overall, these results indicate that Softmax activations for pre-trained LLMs exhibit high redundancies.

Empirical Statistics for the “Depth Factor”. To further support Theorem 3.2 and the claim made in Theorem 3.3, we applied cross-layer sharing to the top layers of LLaMA-3.1 8B and evaluated 100 randomly selected samples from the PMC post-training corpus. The average results of the following terms are: $\|\delta_i\|/\|\mathbf{x}_i\| = 0.070$, $\|J(A_i)\| = 0.041$, and

UniAttn: Reducing Inference Costs via Softmax Unification for Post-Training LLMs

Method	TTFT (s)	KV Cache	Medical				General		
			PubMedQa	MedMCQA	MedQA	AVG	SIQA	CommonsenseQA	AVG
Mistral-7B (w/ GQA)									
Pre-Trained	1.94	100%	75.8	48.3	50.9	58.3	46.7	56.5	51.6
Post-Train	1.94	100%	78.8	49.7	60.3	62.9	53.7	76.6	65.2
LLMDrop-Half	1.54	81.3%	78.0	50.6	<u>59.0</u>	62.5	<u>52.5</u>	74.5	63.5
LLMDrop-Full	1.21	62.5%	79.0	50.2	56.7	62.0	51.8	73.6	62.7
CLA-Half	1.94	81.3%	78.6	<u>56.0</u>	58.5	<u>64.4</u>	52.0	77.9	<u>65.0</u>
CLA-Full	1.91	62.5%	<u>78.8</u>	55.0	55.0	62.9	50.5	75.1	62.8
UniAttn	1.23	81.3%	78.2	57.3	60.5	65.3	53.4	<u>77.5</u>	65.5
Gemma2-9B (w/ GQA)									
Pre-Trained	2.23	100%	78.6	57.6	60.6	65.6	51.5	68.4	60.0
Post-Train	2.23	100%	78.6	58.6	61.9	66.4	54.4	75.6	65.0
LLMDrop-Half	1.94	81.0%	78.6	56.4	<u>60.5</u>	<u>65.2</u>	55.6	68.4	62.0
LLMDrop-Full	1.66	64.3%	78.2	54.8	58.7	63.9	54.8	62.9	58.9
CLA-Half	2.19	78.6%	79.2	<u>56.6</u>	56.3	64.0	53.5	76.0	64.8
CLA-Full	2.24	64.3%	74.0	39.3	38.5	50.6	48.3	51.8	43.4
UniAttn	1.69	82.1%	<u>79.0</u>	60.7	64.3	68.0	53.7	<u>74.4</u>	<u>64.1</u>

Table 10. Post-training performance comparison. **Bold** and underline denote the best and second-best performance of compressed models. For each method, we report their time to first token (TTFT, in seconds) and KV-cache retain rate (KV Cache).

Dataset	Average	Difference Between Top Half and Bottom Half Layers	Max	Min	Standard Deviation
PMC	0.8347	0.1314	0.9729	0.0159	0.1955
Math	0.8243	0.1149	0.9734	0.0384	0.1860
Tulu3	0.8214	0.1212	0.9719	0.0307	0.1896
F15K	0.7927	0.1475	0.9710	0.0033	0.2109

Table 11. Statistics of the cosine similarity of Softmax activations for LLaMA-3.1 8B across different datasets.

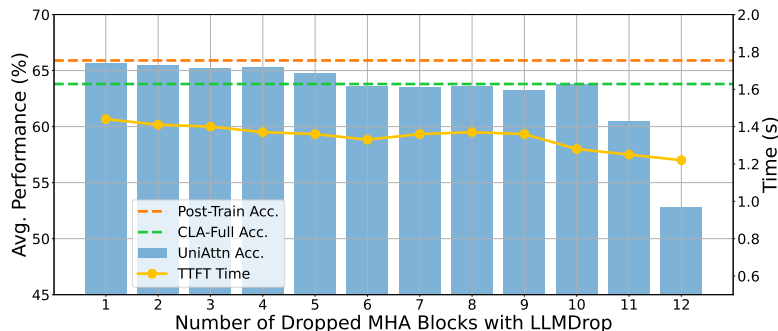


Figure 7. Results on further dropping UniAttn layers (%). We present the average accuracy and time to first token (TTFT) latency under different number of dropped MHA blocks via LLMDrop. Note that we only drop MHA blocks with unified Softmax activations.

$\|J(A_i)\hat{\delta}\|/\|\text{Softmax}(A_i)\| = 0.038$. These results support that (1) δ_i is small comparing to $\|x_i\|$, validating Assumption 3.5; (2) the depth factor is indeed diminished under cross-layer KV-cache sharing, consistent with Proposition 3.6.

Different Compensation Designs. To compare different compensation designs, we attach the input and output of the W_c transformation to different activations. As shown in Table 12, directly compensating the MHA output with its input yields the best results. When adopting “finer compensation granularities”, i.e., positioning the input and output closer together (Rows 3 and 4), post-training performance decreases. Similarly, adopting “coarser compensation granularities”, i.e., moving the output compensation to after the FFN (Row 2), also results in lower performance. These findings suggest that using a linear transformation to compensate for errors specifically within the MHA module is the best-performing approach.

Input to W_c	Output adds to	AVG
MHA input	MHA output	65.4
MHA input	FFN output	64.1
MHA input	Activation before W_o	<u>65.1</u>
Activation projected by W_v	Activation before W_o	64.3

Table 12. Performance comparison (%) of different compensation designs.

Algorithm 1 UniAttn Pipeline

Input: Pre-trained Model M , Post-train dataset D , SuperBlock size b , Apply SuperBlock merging from layer i_s to i_e
 Create UniAttn model M_{uni} by creating $\frac{i_e - i_s + 1}{b}$ SuperBlocks in M
 Sample a subset D_{init} with 1000 samples from D
 For model M , forward all samples from D_{init} , calculate the average output activations \mathbf{x}'_i for each MHA block.
for $i = 1$ **to** $\frac{i_e - i_s + 1}{b}$ **do**
 for $j = 1$ **to** $b - 1$ **do**
 For model M_{uni} , forward all samples from D_{init} , calculate the average output activations $\mathbf{x}'_{\text{uni}, i_s + (i-1)b + j}$ and the average input activations $\mathbf{x}_{\text{uni}, i_s + (i-1)b + j}$ for MHA block in layer $i_s + (i - 1)b + j$.
 Calculate the initialization for the $W_{c, i_s + (i-1)b + j}$ matrix in layer $i_s + (i - 1)b + j$ according to Theorem 3.1.
 Insert the initialized $W_{c, i_s + (i-1)b + j}$ matrix to layer $i_s + (i - 1)b + j$ in model M_{uni} .
 end for
end for
 Freeze all training parameters other than the W_c matrices in M_{uni} . Train W_c with dataset D and apply early stop when loss stops decreasing (we consider the exponential moving average of training loss).
 Conduct full fine-tuning on M_{uni} with D .
Output: Trained UniAttn model M_{uni} .

Experimental Analysis on the Impact of Model Depth. In Section 3.4, we demonstrated that, unlike cross-layer KV sharing methods, UniAttn does not diminish the depth factor in pre-trained LLMs. To provide experimental evidence for this, we further apply LLMDrop to the MHA modules that utilize unified Softmax activations from preceding layers (a total of 12 layers in UniAttn for the LLaMA-3.1 8B model) in post-trained UniAttn models. Specifically, we compute the input-output similarities of these MHA modules and simply prune the top k MHA modules with the highest similarities. The pruned model is then directly evaluated without additional fine-tuning. The average performance w.r.t. k in shown in Figure 7. As shown in the figure, pruning a few MHA modules from our UniAttn model still results in higher performance than the CLA-Full model variant. After pruning 10 MHA modules, UniAttn+LLMDrop achieves an average performance of 63.8, matching the performance of CLA-Full reported in Table 1. This demonstrates that UniAttn better preserves the impact of model depth compared to CLA. Furthermore, we can also conclude that the depth of the model significantly contributes to the post-train performance, thereby validating our theoretical analysis.

D. Pipeline for Applying UniAttn during Post-Training

We provide a detailed pipeline for applying UniAttn as Algorithm 1.

E. Theoretical Insights for Proposing Theorem 3.2

We first give a series of conclusions (namely Theorem E.1, Theorem E.2, Theorem E.3, and Theorem E.4) as preliminaries.

Lemma E.1. *(A linear Pre-Norm system has bounded growth) $f_i : \mathbb{R}^n \rightarrow \mathbb{R}^n$, $i \in \mathbb{N}$ are LINEAR transformations and $\text{Norm}(\cdot)$ yields a vector with unit Frobenius-norm (denoted as $\|\cdot\|$). Let $\mathbf{x}_0 \in \mathbb{R}^n$ be the input to the system. Consider an L -layer Pre-Norm architecture defined by:*

$$\begin{aligned} \mathbf{x}_k &= \mathbf{x}_{k-1} + f_k(\text{Norm}(\mathbf{x}_{k-1})), \\ \text{for } k &= 1, 2, \dots, L. \end{aligned} \quad (10)$$

If the largest singular value in all transformation matrices is bounded by λ , then:

$$\|\mathbf{x}_L\| \leq \|\mathbf{x}_0\| + \lambda L \quad (11)$$

Proof. Unroll the expression of \mathbf{x}_L and inductively:

$$\mathbf{x}_L = \mathbf{x}_0 + \sum_{k=1}^L F_k(\text{Norm}(\mathbf{x}_{k-1})) \quad (12)$$

As $\|\text{Norm}(\mathbf{x}_k)\| = 1$ for all k , then:

$$\begin{aligned} \|\mathbf{x}_L\| &= \left\| \mathbf{x}_0 + \sum_{k=1}^L F_k(\text{Norm}(\mathbf{x}_{k-1})) \right\| \\ &\leq \|\mathbf{x}_0\| + \sum_{k=1}^L \|F_k(\text{Norm}(\mathbf{x}_{k-1}))\| \\ &\leq \|\mathbf{x}_0\| + \sum_{k=1}^L \|\lambda \cdot \text{Norm}(\mathbf{x}_{k-1})\| \\ &= \|\mathbf{x}_0\| + \lambda L \end{aligned} \quad (13)$$

□

Theorem E.1 shows that a Pre-Norm linear system has bounded growth. The norm of output by each layer grows *at most linearly* with depth L .

Proposition E.2. *(Pre-trained LLMs are linear Pre-Norm systems) Pre-trained decoder-based LLMs exhibit a high linearity score. Formally, let $A, B \in \mathbb{R}^{n \times d}$ denote the normalized input and output of a decoder block in LLM, respectively,*

$$\min_X \|AX - B\| \approx 1 \quad (14)$$

Theorem E.2 has been validated by (Razzhigaev et al., 2024) on pre-trained LLMs, suggesting that we can approximate each decoder block by a linear transformation with bounded singular values, thus placing pre-trained LLMs structurally “close” to a linear Pre-Norm system as in Theorem E.1. In the following discussion, we approximate pre-trained LLMs with an equivalent linear Pre-Norm system and investigate its input and output in each layer.

Proposition E.3. *(Pre-trained LLM layers primarily change the magnitude of activations) The input and output of a layer in pre-trained decoder-based LLMs share a high cosine similarity.*

Theorem E.3 has been validated by (Men et al., 2024) on pre-trained LLMs, indicating that each layer in LLMs predominantly change the *magnitude* of the activation. We leverage the following conclusion for analyzing the change of activation magnitude.

Proposition E.4. *(Top layers of Pre-Norm transformers have smaller singular values) Training Pre-Norm transformers leads to top layers receiving smaller updates (gradient norms decrease from bottom to top).*

(Xiong et al., 2020) has given both a theoretical proof sketch and experimental evidence of Theorem E.4. Based on Theorem E.2, we approximate each layer in LLMs as a linear transformation. To further show that the approximated linear transformations of the top layers in Pre-Norm LLMs tend to have smaller singular values, we give the following proof:

Proof. With Theorem E.1 and Theorem E.2, we have shown that pre-trained Pre-Norm LLMs can be approximated as linear Pre-Norm systems. Suppose a pre-trained LLM operates on activations $\mathbf{x} \in \mathbb{R}^d$, each layer i in the pre-trained LLM can be treated as a linear transformation matrix $W_i \in \mathbb{R}^{d \times d}$. A generic gradient-based update can be expressed as:

$$W_i^{t+1} = W_i^0 - \sum_{t=0}^t \eta \nabla_{W_i} \mathcal{L}^t \quad (15)$$

Hence, the norm between initial and final weights satisfies:

$$\|W_i^{t+1} - W_i^0\| \leq \sum_{t=0}^t \|\eta \nabla_{W_i} \mathcal{L}^t\| \quad (16)$$

We denote the singular value decomposition of $W_i^{t+1} - W_i^0$ as $W_i^{t+1} - W_i^0 = U \Sigma V^T$, it is easy to derive that:

$$\begin{aligned} & \|W_i^{t+1} - W_i^0\| \\ &= \sqrt{\text{tr}[(\|W_i^{t+1} - W_i^0\|)(\|W_i^{t+1} - W_i^0\|)^T]} \\ &= \sqrt{\text{tr}(U \Sigma V^T V \Sigma^T U^T)} \\ &= \sqrt{\text{tr}(\Sigma \Sigma^T)} = \sqrt{\sum_{i=1}^d \sigma_i^2} \end{aligned} \quad (17)$$

where σ_i denote the i -th singular value in Σ . Normally, the largest singular value σ_{\max} dominates in the quadratic term, thus we can further write:

$$\|W_i^{t+1} - W_i^0\| = \sqrt{\sum_{i=1}^d \sigma_i^2} \approx \sigma_{\max}(W_i^{t+1} - W_i^0) \quad (18)$$

Based on the basic features of singular values, we can show that:

$$\begin{aligned} \sigma_{\max}(W_i^{t+1}) &\leq \sigma_{\max}(W_i^0) + \sigma_{\max}(W_i^{t+1} - W_i^0) \\ &\leq \sum_{t=0}^t \|\eta \nabla_{W_i} \mathcal{L}^t\| + \sigma_{\max}(W_i^0) \end{aligned} \quad (19)$$

Due to having smaller values of $\|\eta \nabla_{W_i} \mathcal{L}^t\|$ (i.e., smaller gradient norm), compared to earlier layers, the top layers typically have smaller updates on the largest singular value, thus tend to have smaller σ_{\max} values. \square

Since pre-trained LLMs mainly change the magnitude of the activation (as shown in Theorem E.3), we can use the size of the largest singular values in each layer as an indicator of the corresponding activation magnitude change. In Pre-Norm architectures, each layer operates on an input with a constant norm. This leads to the assumption that the top-layer transformations generally generate outputs with smaller norms, which is Theorem 3.2 we propose in the article.

F. Proof for Theorem 3.1

Proof. Solving for the initialization of W_c that incurs minimal compensation error is equivalent to solving the following optimization problem:

$$\min_{W_c} \|\mathbb{E}(\mathbf{x}_{i+b} W_c - \epsilon)\|. \quad (20)$$

v	N/A	1	2	3	4	8	16
PPL	5.914	2.890	2.871	2.835	2.850	2.822	2.837

Table 13. Perplexity results for initializations with different v values on LLaMA-3.1 8B in the medical domain. “N/A” represents applying Softmax Unification without linear projections.

Since we use a small subset of the training dataset (with S samples, we denote this as the *initialization set*) to calculate the initialization, the objective above can be rewritten as:

$$\min_{W_c} \frac{1}{S} \sum_{j=1}^S \|\mathbf{x}_{i+b,j} W_c - \epsilon_j\| \quad (21)$$

This is a Least Absolute Deviations problem, and can be solved with the simplex algorithm, which is NP as shown in (Fearnley & Savani, 2015). To guarantee that the initialization method is efficient even in the worst case, we in turn consider the Least Squares variant:

$$\min_{W_c} \frac{1}{S} \sum_{j=1}^S \|\mathbf{x}_{i+b,j} W_c - \epsilon_j\|^2. \quad (22)$$

The Least Squares variant is a convex optimization problem, and has a closed-form solution as follows:

$$W_c = X^+ E, \quad (23)$$

where X is a matrix created by concatenating all $\mathbf{x}_{i+b,j}$ instances, E is created by concatenating all ϵ_j instances, and X^+ represents the Moore-Penrose inverse of X . When actually calculating for W_c , it is time-consuming to calculate X^+ as the size of X is big. Therefore, we set the *maximum instance size* of X as v . Specifically, we average \mathbf{x} ’s and ϵ ’s for every $\frac{S}{v}$ instances in the initialization set, and calculate W_c on the averaged \mathbf{x} ’s and ϵ ’s. For simplicity, we denote the averaged \mathbf{x} ’s and ϵ ’s as $\mathbb{E}(\mathbf{x}_{i+b})$ and $\mathbb{E}(\epsilon)$. Consequently, the calculation for W_c is formulated as:

$$W_c = V \Sigma^+ U^T \mathbb{E}(\epsilon), \quad (24)$$

where $V \Sigma^+ U^T$ is the Moore-Penrose inverse of $\mathbb{E}(\mathbf{x}_{i+b})$, calculated via SVD. \square

To find an appropriate v value for initialization, we have conducted preliminary experiments on LLaMA-3.1 8B in the medical domain. Specifically, we have benchmarked the perplexity on the *initialization set* after inserting all linear projections with initialized weights calculated. As shown in Table 13, most performance contribution comes from the act of adding initialization, and increasing the number of v affects the PPL values slightly. These experiments guided us to adopt $v = 1$ for our experiments due to its simplicity.

G. Proof for Theorem 3.3

Proof. For simplicity, we suppose \mathbf{x}_{i+1} is already normalized by the Pre-Norm. We can re-write Equation (8) as:

$$\begin{aligned} \mathbf{x}'_{i+1} &= \text{softmax}\left(\frac{\mathbf{x}_{i+1} W_{q,i+1} K_i^T}{\sqrt{d_k}}\right) V_i W_{o,i+1} \\ &\quad + \mathbf{x}_{i+1} \\ &= \text{softmax}\left(\frac{(\mathbf{x}_i + \delta_i) W_{q,i+1} K_i^T}{\sqrt{d_k}}\right) V_i W_{o,i+1} \\ &\quad + \mathbf{x}_{i+1} \\ &= \text{softmax}\left(\frac{\mathbf{x}_i W_{q,i+1} K_i^T}{\sqrt{d_k}}\right) \\ &\quad + \frac{\delta_i W_{q,i+1} K_i^T}{\sqrt{d_k}} V_i W_{o,i+1} + \mathbf{x}_{i+1} \end{aligned} \quad (25)$$

Let $A_i = \frac{\mathbf{x}_i W_{q,i+1} K_i^T}{\sqrt{d_k}}$, $\hat{\delta}_i = \frac{\delta_i W_{q,i+1} K_i^T}{\sqrt{d_k}}$. By expanding Softmax to the first order:

$$\begin{aligned} \mathbf{x}'_{i+1} &= [\text{softmax}(A_i) + J(A_i)\hat{\delta}_i] V_i W_{o,i+1} \\ &+ \mathbf{x}_{i+1} + o(\hat{\delta}_i^2), \end{aligned} \quad (26)$$

where $J(A_i)$ is the Jacobian of Softmax at A_i . We ignore the $o(\hat{\delta}_i^2)$ remainder. (Xiao et al., 2024) has discovered that the pre-trained LLMs generally exhibit an ‘‘attention sink’’ feature, in which self-attentions heavily attend to the ‘‘sink token’’ at the beginning of a sequence. We adopt such feature to estimate $\|J(A_i)\|$. According to the statistical pattern concluded by (Xiao et al., 2024), attention logits $\mathbf{a} \in \mathbb{R}^l$ of a sequence with length l is approximately:

$$a_i = 1 \ (0 < i < d), \ a_j = -1 \ (i \geq d), \ d \ll l \quad (27)$$

(Xiao et al., 2024) empirically adopts $d = 4$. For a sequence of $l = 1024$, $\|J(\text{softmax}(\mathbf{a}))\| \approx 0.03 \ll 1$, and decreases as l increases. Therefore, we can conclude that the coefficient of the $\hat{\delta}$ term is significantly smaller than that of the Softmax term, making the contribution of the ‘‘depth factor’’ negligible. \square

H. Proof for Theorem 3.4

Proof. In the forward pass of UniAttn:

$$\begin{aligned} \mathbf{x}'_{i+1} &= s_i(\mathbf{x}_{i+1} W_{v,i+1}) W_{o,i+1} + \mathbf{x}_{i+1} \\ &= s_i(\mathbf{x}_i + \delta_i) W_{v,i+1} W_{o,i+1} + \mathbf{x}_{i+1} \end{aligned} \quad (28)$$

Observing that LLM layers primarily change activation magnitudes (see Theorem E.3), we assume \mathbf{x}_i and δ sharing similar directions, further leading to $\frac{\|s_i \mathbf{x}_i W_{v,i+1} W_{o,i+1}\|}{\|s_i \delta_i W_{v,i+1} W_{o,i+1}\|} \approx \frac{\|\mathbf{x}_i\|}{\|\delta_i\|}$. Self-attention in UniAttn maintains the relative magnitude of the depth factor, ensuring its influence on the output. \square

I. More Insights on Linear Compensation

To demonstrate the effectiveness of our linear compensation strategy, we propose the following theorem:

Theorem I.1. $A, B \in \mathbb{R}^{m \times n}$, $X \in \mathbb{R}^{n \times n}$. Suppose that each element from A and B are drawn from a Gaussian distribution such that $a_{ij}, b_{ij} \sim N(0, 1)$. It satisfies that:

$$\mathbb{E}[\min_X \|AX - B\|] = \begin{cases} \sqrt{n(m-n)}, & \text{if } m \geq n, \\ 0, & \text{if } m < n. \end{cases} \quad (29)$$

See the following subsections for the proof. In the article, we apply the F15K dataset (Su, 2023) to calculate the error ϵ on LLaMA-2 7B (Touvron et al., 2023) and LLaMA-3.1 8B (Dubey et al., 2024) models after inserting the initialized linear transformation W_c according to Theorem 3.1. While the sequence length being $m = 5120$ and the hidden size of applied models being $n = 4096$, the error is 11.09 and 5.76 after linear compensation, correspondingly, which are both *magnitudes lower* than their expectations on random data. Those results demonstrate the effectiveness of our linear compensation strategy.

We give the proof for Theorem I.1 in the following subsections.

I.1. Preliminaries

To prove Theorem I.1, we adopt the notations in Theorem I.1 and prove a series of lemmas first.

Lemma I.2. Let $P = AA^+$, P is an orthogonal projection and $\text{Im}(P) = \text{Col}(A)$.

Proof. The Moore-Penrose inverse matrix exhibits some basic features, namely $AA^+A = A$ and $(AA^+)^T = AA^+$. Using that feature we can easily verify that:

$$P^2 = AA^+AA^+ = (AA^+A)A^+ = AA^+ = P \quad (30)$$

$$P^T = (AA^+)^T = AA^+ = P \quad (31)$$

So P is an orthogonal projection.

Next, we prove $\text{Im}(P) = \text{Col}(A)$. For any vector $\mathbf{v} \in \text{Col}(A)$, there exists a $\mathbf{c} \in \mathbb{R}^n$ that $\mathbf{v} = A\mathbf{c}$. We have:

$$P\mathbf{v} = AA^+A\mathbf{c} = (AA^+A)\mathbf{c} = A\mathbf{c} = \mathbf{v} \quad (32)$$

So $\mathbf{v} \in \text{Im}(P)$. Therefore, $\text{Col}(A) \subseteq \text{Im}(P)$. Since $P = AA^+$, it is obvious that $\text{Im}(P) \subseteq \text{Col}(A)$. Hence, we can conclude that $\text{Im}(P) = \text{Col}(A)$. \square

Lemma I.3. $I - P$ is an orthogonal projection and $\text{Im}(I - P) = \text{Col}(A)^\perp$.

Proof. First, we prove that $I - P$ is an orthogonal projection:

$$(I - P)^2 = I - 2P + P^2 = I - 2P + P = I - P \quad (33)$$

$$(I - P)^T = I - P^T = I - P \quad (34)$$

Then, we prove that $\text{Im}(I - P) = \text{Col}(A)^\perp$. For any $\mathbf{v} \in \text{Im}(I - P)$, there exists a $\mathbf{c} \in \mathbb{R}^m$ that $\mathbf{v} = (I - P)\mathbf{c}$. Let $\mathbf{d} \in \text{Col}(A)$, then there exists a $\mathbf{w} \in \mathbb{R}^n$ that $\mathbf{d} = A\mathbf{w}$. Computing the inner product of \mathbf{v} and \mathbf{d} yields:

$$\begin{aligned} \langle \mathbf{v}, \mathbf{d} \rangle &= \langle (I - P)\mathbf{c}, A\mathbf{w} \rangle = \langle \mathbf{c}, (I - P)A\mathbf{w} \rangle \\ &= \langle \mathbf{c}, (A - AA^+A)\mathbf{w} \rangle = \langle \mathbf{c}, \mathbf{0} \rangle = 0 \end{aligned} \quad (35)$$

This shows that $\mathbf{v} \in \text{Col}(A)^\perp$, and in turn $\text{Im}(I - P) \subseteq \text{Col}(A)^\perp$.

Conversely, suppose $\mathbf{u} \in \text{Col}(A)^\perp$. Recall Theorem I.2 that P is an orthogonal projection and $\text{Im}(P) = \text{Col}(A)$, we have $P\mathbf{u} = \mathbf{0}$. Therefore,

$$(I - P)\mathbf{u} = \mathbf{u} - P\mathbf{u} = \mathbf{u} \quad (36)$$

This shows that $\mathbf{u} \in \text{Im}(I - P)$, and in turn $\text{Col}(A)^\perp \subseteq \text{Im}(I - P)$. Therefore, $\text{Im}(I - P) = \text{Col}(A)^\perp$. \square

From Theorem I.3, we can immediately conclude that:

Corollary I.4. $\text{rank}(I - P) = m - \min(m, n)$

Proof. $\text{rank}(I - P) = \dim \text{Im}(I - P) = \dim \text{Col}(A)^\perp = m - \text{rank}(A)$. Recall Theorem I.1 that every element from A is sampled from a Gaussian distribution, so that by probability of 1 we have $\text{rank}(A) = \min(m, n)$, which leads to the conclusion of this corollary. \square

Lastly, we give a lemma on orthogonal projections to a Gaussian-sampled vector:

Lemma I.5. If $\mathbf{b} \sim N(\mathbf{0}, I_{m \times m})$ is a standard Gaussian in \mathbb{R}^m and Q is an orthogonal projector of rank k , then

$$\mathbb{E}[\|Q\mathbf{b}\|] = \sqrt{k} \quad (37)$$

Proof. $\mathbb{E}[\|Q\mathbf{b}\|^2] = \mathbb{E}[\mathbf{b}^T Q^T Q \mathbf{b}] = \mathbb{E}[\mathbf{b}^T Q \mathbf{b}] = \mathbb{E}[\text{tr}(\mathbf{b}^T Q \mathbf{b})] = \mathbb{E}[\text{tr}(Q \mathbf{b} \mathbf{b}^T)] = \text{tr}(Q \mathbb{E}[\mathbf{b} \mathbf{b}^T])$. As $\mathbf{b} \sim N(\mathbf{0}, I_{m \times m})$, $\mathbb{E}[\mathbf{b} \mathbf{b}^T] = I$. Therefore, using the trace property of projectors:

$$\text{tr}(Q \mathbb{E}[\mathbf{b} \mathbf{b}^T]) = \text{tr}(Q) = k \quad (38)$$

In turn, we can conclude that $\mathbb{E}[\|Q\mathbf{b}\|] = \sqrt{k}$. \square

I.2. Proof

Finally, we give the proof for Theorem I.1.

Proof. According to Theorem 3.1, for given A and B , the optimal solution X^* that satisfies $\|AX^* - B\| = \min_X \|AX - B\|$ is given by:

$$X^* = A^+B, \quad (39)$$

where A^+ is the Moore-Penrose inverse of A . We can re-write the objective as:

$$\begin{aligned} \mathbb{E}(\|AA^+B - B\|^2) &= \mathbb{E}(\|(I - AA^+)(-B)\|^2) \\ &= \mathbb{E}(\|(I - AA^+)B\|^2) \\ &= \sum_{i=1}^n \mathbb{E}(\|(I - AA^+)\mathbf{b}_i\|^2) \end{aligned} \quad (40)$$

According to Theorem I.3 and Theorem I.4, $I - AA^+$ is an orthogonal projection and $\text{rank}(I - AA^+) = m - \min(m, n)$. With Theorem I.5, we know that for any i , $\mathbb{E}(\|(I - AA^+)\mathbf{b}_i\|^2) = m - \min(m, n)$. Therefore, we can conclude that:

$$\mathbb{E}(\|AA^+B - B\|^2) = \begin{cases} n(m - n), & \text{if } m \geq n, \\ 0, & \text{if } m < n. \end{cases} \quad (41)$$

which leads to the conclusion in Theorem I.1. □